International Soil and Water Conservation Research xxx (xxxx) xxx

Contents lists available at ScienceDirect

International Soil and Water Conservation Research

journal homepage: www.elsevier.com/locate/iswcr

Original Research Article

Evaluating black soil thickness under straw return practices by using ground penetrating radar

Chang Liu [a], Gang Liu [a,b,*], Chenxi Dan [a], Ya Liu [a], Qiong Zhang [a], Han Luo [a], Chutian Zhang [a], Zhen Guo [c], Kaishan Song [d]

[a] State Key Laboratory of Soil and Water Conservation and Desertification Control, College of Soil and Water Conservation Science and Engineering (Institute of Soil and Water Conservation), Northwest A&F University, Yangling, 712100, China
[b] Institute of Soil and Water Conservation of Chinese Academy of Sciences and Ministry of Water Resources, Yangling, 712100, China
[c] Sichuan Huabiaoce Testing Technology Co. Ltd., Chengdu, 610097, China
[d] The Northeast Institute of Geography and Agricultural Ecology, Chinese Academy of Sciences, Jilin, 130102, China

ARTICLE INFO

Article history:
Received 1 December 2025
Received in revised form
3 February 2026
Accepted 6 February 2026
Available online xxx

Keywords:
Ground penetrating radar
Black soil thickness
Straw return
Soil permittivity

ABSTRACT

The intensive utilization and erosion-induced thinning of global black soil threaten its sustainable use, making accurate thickness assessment crucial. This study aimed to evaluate the impact of straw return practices on the accuracy of Ground Penetrating Radar (GPR) for measuring black soil thickness. Indoor simulation experiments were conducted with varying soil bulk density (1.1 g cm^{-3}, 1.3 g cm^{-3}, and 1.5 g cm^{-3}), moisture contents (10 %, 20 %, 30 %), and straw application methods (mulched or incorporated at 50 % and 100 % rates). The results indicated that soil permittivity generally increased with moisture under both straw treatments. While permittivity increased with bulk density under straw mulching, it responded variably under incorporation (slight increase at 50% rate but decrease at 100 %). GPR overall achieved an accuracy of 86.5 %–93.8 %. It proved effective under straw-incorporated conditions,but had limited effectiveness under low bulk density and moisture content in the straw-mulched treatment. Field measurements revealed average thicknesses of 29.1 cm (bare slope), 28.6 cm (straw-mulched slope), and 34.6 cm (straw-incorporated slope), with distinct distribution patterns along slopes. This study clarified the applicable range and precision of GPR for measuring black soil thickness under straw return and provided scientific and technological support for sustainable black soil management.

1. Introduction

Black soil is acknowledged as one of the most fertile soil types worldwide (Sorokin et al., 2021). It spans approximately 916 million hectares globally, with the predominant portion dedicated to agricultural production, while a smaller fraction remains under grassland and forest cover (Eckmeier et al., 2007; Labaz et al., 2018). This soil type holds significant economic and strategic importance for global food security (Rosegrant & Cline, 2003). In the context of a growing global population and nearly 900 million individuals facing food insecurity, the relevance of black soil has become increasingly pronounced (Tong et al., 2017). Furthermore, as a vital terrestrial carbon reservoir and a core component supporting food security, the black soil thickness and distribution area directly affect both soil productivity and its capacity for carbon sequestration (Labaz et al., 2024; Xie et al., 2023). The fertile black soil of China is primarily concentrated in the northeast region, constituting one of the four major black soil regions over the world. This vital soil resource contributes to a quarter of Chinese total grain production (Wang et al., 2024). Nevertheless, the synergy of prolonged intensive cultivation, unsustainable land use practices, and climate change has precipitated several significant challenges, including a decline in organic matter content, an expansion of erosion areas, diminished soil productivity, and ecological degradation (Sui & Dai, 2025). Since large-scale

* Corresponding author. Institute of Soil and Water Conservation, Northwest A&F University, No. 26, Xinong Road, Yangling, Shaanxi Province, 712100, China.
E-mail address: gliu@foxmail.com (G. Liu).

Peer review under the responsibility of International Research and Training Center on Erosion and Sedimentation, the China Water and Power Press, and China Institute of Water Resources and Hydropower Research.

https://doi.org/10.1016/j.iswcr.2026.100636

agriculture in the black soil region of China in the 1950s, severe soil erosion has resulted in an average reduction of black soil thickness by 40 cm (Wang et al., 2022a). The current regional average erosion rate is estimated to be around 15,000 kg ha^{-1} yr^{-1} or higher (Nearing et al., 2017). This dual degradation in quantity and quality of black soil not only threatens regional agricultural sustainability but also poses systemic risks to national food security and ecological stability.

Conventional tillage methods employed in traditional agricultural systems result in considerable degradation of land resources, posing a substantial threat to soil stability and its capacity for water retention (Sui & Dai, 2025). The soil degradation associated with these traditional farming practices has emerged as a global issue, directly impairing the sustainability potential of agriculture (Li et al., 2025). Conservation tillage, which originated in North America, has been adopted in over 70 countries. It covers approximately 180 million hectares, accounting for 12.5 % of the global arable land area (Xiao et al., 2021). The conservation of black soil, aimed at improving soil health, relying on conservation tillage management systems such as no-tillage, reduced tillage, subsoiling, and straw mulching (Sun et al., 2020). It has been proven effective in reducing soil erosion, enhancing organic matter content, and improving soil water-thermal conditions (Lal, 2013; Kassam et al., 2019). Specifically, reduced tillage sowing mitigates disruption to soil structure by decreasing the frequency of traditional tillage and employing a specialized planter to complete agricultural operations in a single pass (Zhang et al., 2015). Another key measure is straw return, which involves retaining crop residues on the soil surface or incorporating them into the shallow soil layer at a specific ratio after harvest (Kan et al., 2020). During the decomposition of straw, abundant carbon sources are provided for soil microorganisms, thereby stimulating microbial activity and accelerating the decomposition and release of organic nutrients from crop residues (Zhang et al., 2024). Meanwhile, the cementing effect of humus promotes the formation of soil aggregate structure, enhancing aggregate stability (Wu et al., 2024). Furthermore, the physical barrier effect of the straw layer reduces raindrop splash energy, resulting in a reduction of surface runoff by 20 %–60 % and effectively suppressing soil erosion by increasing infiltration (Yang et al., 2021). Currently, two types of straw return modes are primarily employed in the black soil region of China: one is surface mulching return with varying fragment lengths, and the other is soil incorporation with differing pulverization degrees and burial depths (Song et al., 2024). These two returning modes may exert differential impacts on the propagation path and reflection characteristics of Ground Penetrating Radar (GPR) signals. Therefore, there is an urgent need to investigate the applicability of GPR technology in measuring black soil thickness under different returning measures.

GPR represents a highly efficient geophysical method for shallow subsurface investigation (Jonard et al., 2013). As technological advancements continue to unfold and research deepens, GPR reveals promising application prospects across various domains, including geological exploration, water conservancy engineering, and civil engineering. Marecos et al. (2017) reported that GPR serves as an effective tool for determining the thickness of asphalt and granular layers, emphasizing its importance for continuous evaluation of existing pavement structures. Additionally, GPR can also enhance the imaging quality and feature identification capability of underground archaeological remains (Ebraheem et al., 2025). Multiple cross-regional investigations have demonstrated that GPR estimates soil moisture content in vertical profiles using electromagnetic reflection signals from different soil layers (Steelman & Endres, 2012; Koyama et al., 2017). Currently, ground-penetrating radar, leveraging its non-destructive and efficient detection advantages, demonstrates superior performance in homogeneous soil profile detection (Pathirana et al., 2024). Zhang et al. (2018) mapped the spatial distribution of soil depth in grassland ecosystems by using GPR and GIS. Liu et al. (2021) measured the thickness of the black soil on typical slopes in the black soil region in Northeast China. However, the feasibility and accuracy of GPR in measuring the thickness of black soil on sloping farmland with straw mulching and straw incorporation remain unclear. First, it is essential to determine whether the disparity in dielectric properties between the straw cover layer or the crushed and mixed layer and the underlying black soil parent material is sufficiently pronounced. Second, there is an interference effect of the loose structure of the straw layer on the radar signal feature extraction. These two aspects constitute the key scientific issues for GPR technology to accurately identify the black soil layer boundary.

Therefore, this study focused on the typical black soil of Northeast China, aiming to achieve the following objectives: (1) to determine the variation characteristics of soil permittivity under straw-mulched and straw-incorporated conditions through indoor simulation experiments; (2) to evaluate the feasibility of GPR in measuring black soil thickness under straw return conditions and assess accuracy through the analysis of field-measured data. This study provides data support for the technical improvement of GPR for estimating black soil thickness and promotes the precise application of GPR in complex farmland environments. The results are of great significance for the protection and sustainable utilization of black soil resources.

2. Materials and methods

2.1. Study areas

The study area was located in Lishu County, Siping City, Jilin Province (43°21′01″–43°21′39″ N, 124°20′40″–124°21′18″ E), characterized by a temperate semi-humid continental monsoon climate with concurrent periods of rainfall and heat, and relatively sufficient sunlight and precipitation during the crop growing season. The region receives an average annual precipitation of 577 mm, with precipitation primarily concentrated from June to August. The region is characterized by intense and concentrated summer rainfall, cold winters with low temperatures, and an average annual temperature of 6.4 °C. Lishu County contains a variety of soil types influenced by factors including geographical location and soil composition. The predominant soil types found in the cultivated lands are black soil, meadow soil, and chernozem, comprising 23.4 %, 20.8 %, and 18.4 % of the total cultivated area, respectively. Within the study area, the soil was identified as black soil, distinguished by a sandy clay loam texture. The black soil in this study was classified as a Mollisol (Agriboroll group) in the USDA Soil Taxonomy (Soil Survey Staff, 2010, p. 338).

2.2. Experimental design

2.2.1. Indoor experiments

We initially performed controlled laboratory simulations to examine variations in soil dielectric properties under varying conditions. The primary measurement method utilized was GPR (SIR-4000, GSSI, USA), whose detection capability is based on fundamental physical principles: GPR emits electromagnetic waves into the subsurface through its antenna, with the propagation behavior of these waves predominantly influenced by the dielectric permittivity of the material. Variations in permittivity at interfaces between different media result in wave reflections (Persico, 2014). By analyzing the two-way travel time and amplitude of the reflected signals, it is possible to infer the depth and characteristics of subsurface features. Consequently, this indoor experiment was conducted to systematically assess the variations in the dielectric permittivity of black soil subjected to two conservation tillage practices, straw mulching and straw incorporation, across different soil moisture contents and bulk density conditions.

The indoor experiment was conducted with two boxes (2 m length, 1 m width, and 0.3 m height). Additionally, a hollow iron pipe (60 cm long, 3 cm diameter) was placed at the bottom of each box (Fig. 1). Soil bulk densities were set at 1.1 g cm^{-3}, 1.3 g cm^{-3}, and 1.5 g cm^{-3}, and soil moisture contents were set at 10 %, 20 %, and 30 % based on field surveys. Additionally, five different straw return experimental treatments were also established: bare soil (no straw), 50 % straw-mulched, 100 % straw-mulched, 50 % straw-incorporated, and 100 % straw-incorporated. Maize straw was cut into fragments ranging from 5 to 10 cm in length. Prior to the commencement of the experiments, the cut straw was thoroughly homogenized. The application rate for the complete straw return was established at 1.0 kg m^{-2}. In this experiment, maize straw was used for the return treatments. Based on repeated field investigations of the surface straw moisture content during the autumn return period in the study area, the straw moisture content in each experimental group was controlled at 18 % ± 1.33 % through a series of steps including oven-drying, rewetting, and equilibration. The tested soil was sieved through a 5 mm sieve to remove stones and plant residues. Subsequently, the 30 cm boxes were evenly filled with three 10 cm thick layers of this soil according to the preset soil bulk density. Each layer underwent thorough compaction to guarantee homogeneity and structural continuity of the soil. After the boxes were filled, the soil was left to stand for 24 h to allow for natural settlement and formation of a stable soil structure.

Initially, for the first set of treatments, the objective was to clarify the effects of soil moisture content and straw return methods on the soil permittivity. Therefore, soil bulk density was maintained at 1.3 g cm^{-3}, while soil moisture content was varied across three levels (10 %, 20 %, and 30 %) in conjunction with five distinct treatment methods, resulting in a total of 15 treatment combinations. The second set of treatments aimed to examine the

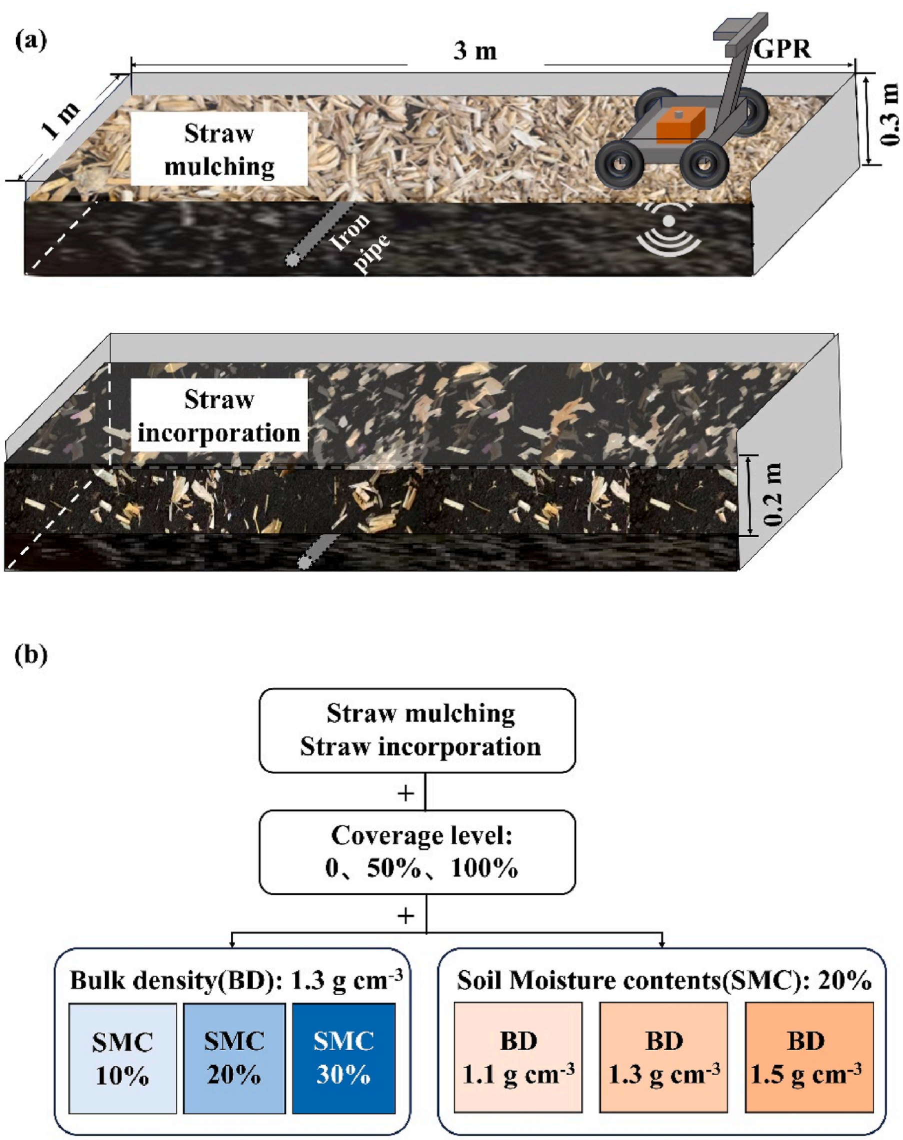

Fig. 1. Indoor experimental design: (a) layout of the two straw return practices; (b) schematic of processing method.

influence of soil bulk density and straw return techniques on the dielectric constant. Soil moisture content was kept constant at 20 %, with variations in soil bulk density (1.1 g cm^{-3}, 1.3 g cm^{-3}, 1.5 g cm^{-3}) and 5 treatment methods, yielding a total of 15 treatment combinations. Consequently, this experiment included a total of 30 treatment combinations, each replicated three times. The clay, silt, and sand contents of the tested black soil were 22.4 %, 39.3 %, and 38.3 %, respectively. Meanwhile, to compare the permittivity of black soil and loess parent material, another set of simulation experiments was designed. With bulk densities set at 1.1 g cm^{-3}, 1.3 g cm^{-3}, and 1.5 g cm^{-3}, and moisture contents at 10 %, 20 %, and 30 %, from which five cross-combinations were configured. Among these, the clay, silt, and sand contents of the tested loess parent material were 20.1 %, 52.6 %, and 27.3 %, respectively. In our experiment, a 400 MHz antenna was employed, utilizing 512 points per scan, a sampling time window of 50 ns, and a scanning rate of 100 scan m^{-1}. Given the specified time window and the number of sampling points per scan, the resultant sampling frequency was determined to be 10.24 GHz. The antenna-ground coupling was achieved through air coupling.

2.2.2. Field experiment

In the study area, three sloping croplands with different conservation tillage practices were selected: a bare land without straw cover, measuring 180 m in length and 70 m in width; a straw-mulched slope spanning 170 m in length and 70 m in width; and a straw-incorporated slope measuring 140 m in length and 60 m in width. These three sloping croplands were cultivated with corn. The straw-mulched slope treatment involved the complete return of straw at an application rate of 9000 kg ha^{-1}, whereas the straw-incorporated slope had a straw return amount of 4000 kg ha^{-1}. Within each study area, three survey lines were evenly distributed according to the slope width (Fig. 2). The GPR survey was conducted from the upper slope to the toe-slope. Additionally, traditional soil profile excavation was employed for validation. At each survey line, one excavation site was selected to conduct actual measurements of the black soil depth (Fig. 2). To verify the accuracy of these measurements, iron pipes were installed perpendicular to the survey line. These iron pipes, measuring 60 cm in length and 3 cm in diameter, were placed specifically at the boundary between the black soil and loess parent material. GPR surveys were conducted using a 400 MHz antenna combined with the profile method. The field experiment was carried out subsequent to the autumn crop harvest in late October. Data acquisition occurred under clear, rain-free daytime conditions, with an average ambient temperature of approximately 5 °C. Soil moisture levels were moderate, the soil remained unfrozen, and the terrain was relatively level.

2.3. Data processing

Electromagnetic wave propagation velocity in soil, calculated based on the target depth obtained from radar images and two-way travel time, can be expressed by the following equation:

$$v = \frac{2h}{t} \tag{1}$$

where v is the propagation velocity of the electromagnetic wave in the medium (m ns^{-1}); h is the depth of the underground target (m); and t is the two-way travel time of the reflected electromagnetic wave signal in the medium (ns).

Based on the electromagnetic wave propagation velocity, the soil permittivity can be calculated using the following equation:

$$\varepsilon = \left(\frac{c}{v}\right)^2 \tag{2}$$

where ε is the soil permittivity; v is the propagation velocity of electromagnetic waves in the medium (m ns^{-1}); and c is the propagation velocity of electromagnetic waves in a vacuum (3×10^8 m s^{-1}).

The mean detection accuracy of the GPR was determined by comparing the actual burial depths of the iron pipes with the corresponding detection depths obtained from the GPR, as expressed by the following formula:

$$RE = \frac{|H - h|}{H} \times 100\% \tag{3}$$

$$AC = 100\% - RE \tag{4}$$

where RE is the relative error (%); AC is the accuracy (%); H is the actual depth (cm); and h is the GPR measured depth (cm). The average accuracy ($\overline{AC}$) is calculated from the AC of each sample point. Additionally, the accuracy range of GPR in determining black soil thickness consists of the maximum and minimum values of the aforementioned AC.

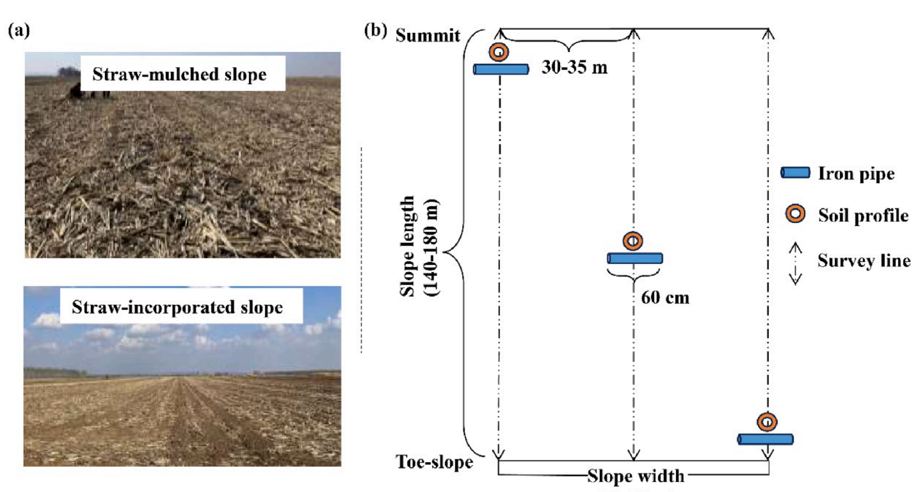

Fig. 2. Schematic of the field experimental design: (a) slope with straw returning treatment; (b) layout of GPR survey lines and markers.

In this study, the Origin 2023 software (OriginLab, USA) was employed to plot the variation diagrams of soil permittivity under different treatments and the characteristic variation maps of black soil thickness on slopes under different tillage practices. Using SPSS 22.0 software, the data were preprocessed by conducting normality tests and homogeneity of variance tests, followed by a multi-factor analysis of variance (ANOVA) on soil permittivity of different treatments ($\alpha < 0.05$). A structural equation model (SEM) was constructed using the "Lavaan" package to investigate the key mechanisms affecting the soil permittivity, and 2000 bootstrap replications were used to calculate the path coefficients at the 0.05 significance level. All radar data were processed using RADAN7 software (GSSI, USA). The workflow included time-zero correction (to eliminate air waves), background removal (to suppress horizontal noise), and gain adjustment (to enhance signals from deeper layers), ensuring the authenticity and clarity of the depth profile (Afshar et al., 2017).

3. Results

3.1. Variation of soil permittivity under different straw return conditions

Soil permittivity under different gradient experimental conditions (including bulk density, moisture content, straw-mulched, and straw-incorporated) was obtained from indoor simulation experiments (Fig. 3). For the bare slope without straw, the permittivity demonstrated a positive correlation with increases in both soil moisture content and bulk density. The variation pattern of the soil permittivity observed in the straw-mulched slope aligned with that of the bare slope. On the straw-incorporated slope, the permittivity demonstrated an increasing trend corresponding to increases in soil moisture content. Conversely, as soil bulk density increased, the variation trends in the soil permittivity diverged depending on the straw returning amount applied to the slope: specifically, the soil permittivity of the slope with 50 % straw-incorporated exhibited a modest increase, whereas that of the slope with 100 % straw-incorporated experienced a slight decrease.

A variance analysis was performed on soil bulk density, soil moisture content, straw-mulched rate, straw-incorporated rate, and soil permittivity, with the dataset categorized into four distinct groups (Fig. 4). Under the condition of straw-mulched with soil moisture content maintained at 20 %, significant differences in soil permittivity were observed between the bare slope and the straw-mulched slope. However, no significant differences were observed between straw-mulched rates of 50 % and 100 %. When the bulk density was maintained at 1.3 g cm^{-3}, no significant variations in soil permittivity were observed between the bare slope and the straw-mulched slope under moisture content levels of 20 % and 30 %. Notably, significant differences in dielectric constant only existed between the bare slope and the fully straw-mulched slope at the low moisture content of 10 %. Under the incorporated straw condition, when the soil moisture content was maintained at 20 %, significant variations in the soil permittivity were observed between the bare slope and the straw-incorporated slope under bulk densities of 1.3 g cm^{-3} and 1.5 g cm^{-3}. In contrast, at a lower bulk density of 1.1 g cm^{-3}, the straw returning amount had no effect on soil permittivity. When the bulk density was maintained at 1.3 g cm^{-3}, there was no significant difference in soil permittivity between the bare slope and the straw-incorporated slope for the low moisture content of 10 %. However, significant differences were evident under all other tested conditions.

To examine the relationship between soil permittivity and multiple influencing variables, this study focused on four specific factors: soil moisture content, bulk density, straw mulching rate, and straw incorporation rate. The findings derived from the SEM analysis are presented in Fig. 5. Under the conditions of straw mulching, soil bulk density and moisture content exhibited direct and statistically significant positive impacts on the permittivity, with path coefficients of 0.33 and 0.68, respectively. These effects were more pronounced than those associated with the rate of

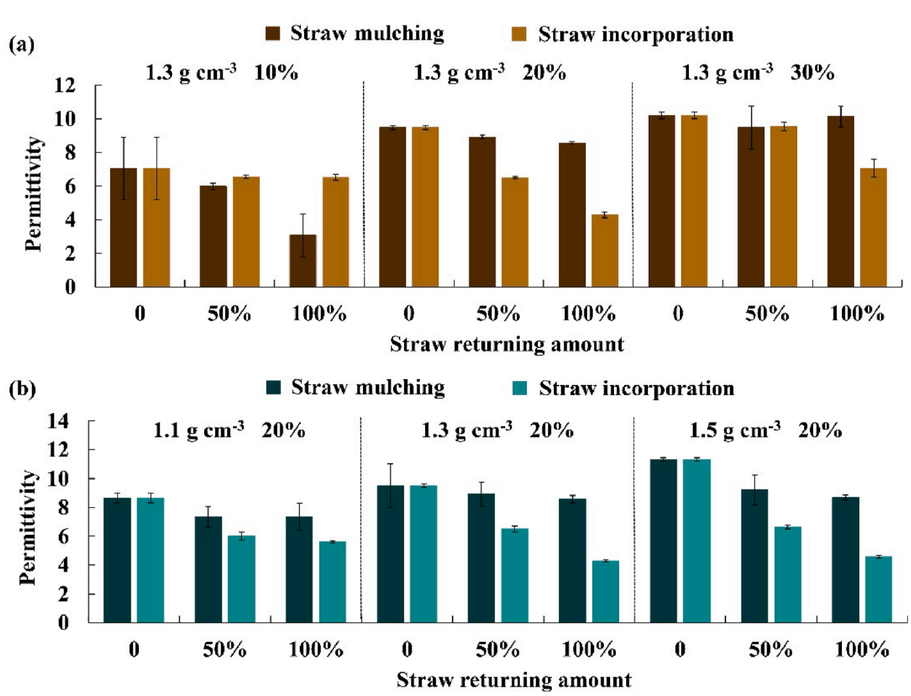

Fig. 3. Permittivity of black soil at varying (a) straw-mulched levels, and (b) straw-incorporation levels.

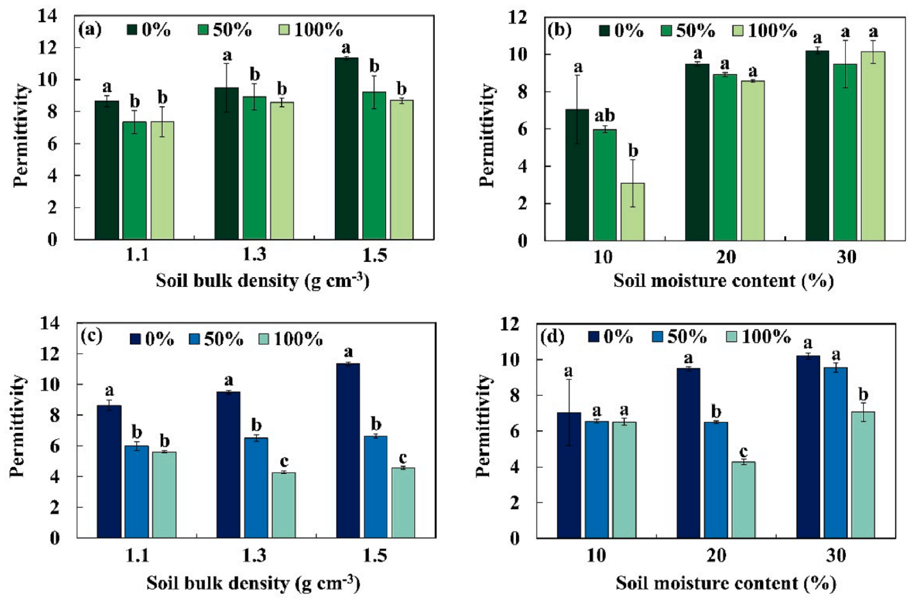

Fig. 4. Variation of soil permittivity with bulk density and moisture content across different straw return conditions. Using one-way ANOVA within the same groups of bulk density and moisture content, different letters indicate significant difference among treatments at 0.05 level.

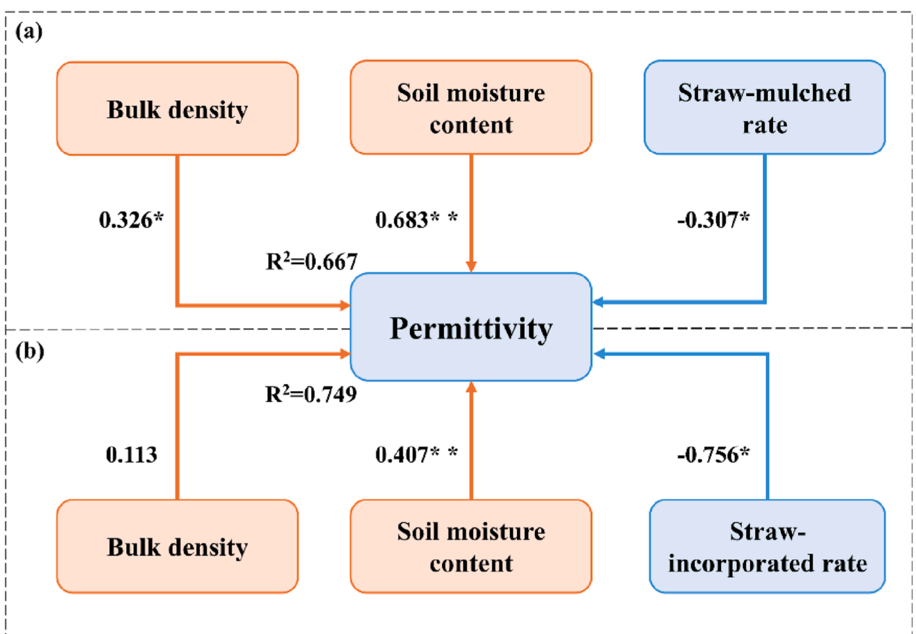

Fig. 5. Path of structural equation model. ** represents $p < 0.01$, and * represents $p < 0.05$.

straw mulch application. The rate of straw mulch exhibited a statistically significant negative impact on permittivity, as indicated by a path coefficient of −0.31. Under conditions involving straw incorporation, soil moisture content exhibited a direct and statistically significant positive influence on permittivity, as indicated by a path coefficient of 0.41. In contrast, the impact of soil bulk density on permittivity was not significant. The rate of straw incorporation exhibited a significant negative impact on permittivity, as indicated by a path coefficient of −0.76. Moreover, its effect was more pronounced than that of the soil moisture content.

3.2. Evaluating the precision of GPR

A fundamental requirement for the identification of black soil thickness using GPR is a pronounced contrast in permittivity. In our study, the permittivity of loess parent material and black soil were determined under varying conditions of bulk density and moisture content through experiments (Table 1). A comprehensive comparative analysis was conducted to evaluate the differences in permittivity among bare black soil slope (BS), 50 % straw-mulched slope (50 % SM), 100 % straw-mulched slope (100% SM), 50 % straw-incorporated slope (50 % SI), 100 % straw-incorporated slope (100 %

Table 1
Soil permittivity of black soil and loess parent material.

Treatment	LPM	BS	50 % SM	100 % SM	50 % SI	100 % SI
A	7.4 ± 0.1b	8.7 ± 0.3a	7.3 ± 0.7b	7.4 ± 0.9b	6.0 ± 0.3c	5.6 ± 0.1c
B	7.8 ± 0.2d	9.5 ± 0.1a	8.9 ± 0.1b	8.6 ± 0.1c	6.5 ± 0.1e	4.3 ± 0.2f
C	9.5 ± 0.1b	11.3 ± 0.1a	9.2 ± 1.0b	8.7 ± 0.2c	6.6 ± 0.1d	4.6 ± 0.1e
D	4.5 ± 0.3bc	7.0 ± 1.8a	6.0 ± 0.2ab	3.1 ± 1.3c	6.6 ± 0.1a	6.5 ± 0.2a
E	8.7 ± 0.4b	10.2 ± 0.2a	9.5 ± 1.3ab	10.1 ± 0.6a	9.6 ± 0.3ab	7.1 ± 0.5c

Note: Group A: bulk density of 1.1 g cm^{-3}, moisture content of 20 %; Group B: bulk density of 1.3 g cm^{-3}, moisture content of 20 %; Group C: bulk density of 1.5 g cm^{-3}, moisture content of 20 %; Group D: bulk density of 1.3 g cm^{-3}, moisture content of 10 %; Group E: bulk density of 1.3 g cm^{-3}, moisture content of 30 %. LPM: loess parent material; BS: bare slope; SM: straw-mulched slope; SI: straw-incorporated slope. Within each row, differing letters denote statistically significant differences at the 95 % confidence level.

SI), and loess parent material (LPM). The analysis demonstrated a significant difference in permittivity between black soil and loess parent material on bare slopes. On slopes with 50 % straw mulch, a difference was detected exclusively under moderate conditions of bulk density (1.3 g cm^{-3}) and moisture content (20 %). Conversely, no significant difference was observed on slopes with 100 % straw mulch when subjected to low bulk density (1.1 g cm^{-3}) and low moisture content (10 %). For slopes with 50 % straw incorporation, the absence of a significant difference was limited to conditions of high bulk density (1.5 g cm^{-3}) and high moisture content (30 %). In contrast, slopes with 100% straw incorporation exhibited a significant difference across all five tested combinations of bulk density and moisture content. Moreover, as illustrated in Fig. 6, an increase in bulk density (Groups A, B, C) corresponded with a progressive amplification in the disparity of permittivity between the black soil and the loess parent material across the various treatments, with the 100 % straw-incorporated slope demonstrating the most significant variation. Conversely, as moisture content increased (Groups D, B, E), the difference in permittivity tended to diminish. The actual burial depths of iron pipes on each slope were determined through field-excavated profiles, with the measured depths being extracted from radar imagery. The actual burial depths of the iron pipes and the measured depths by GPR at the top, middle, and bottom positions of the three slopes are shown in Table 2. For each validation profile, the measurement accuracy of each profile was calculated according to Eq. (3) and Eq. (4). The depth measurement accuracy of the GPR varies with different slope treatment methods. The measurement accuracy is highest for bare soil slopes, ranging from 95 % to 97.7 %. In contrast, whether straw mulching or straw incorporation is applied, higher errors are observed, with measurement accuracy ranging from 86.5 % to 93.8 %. However, statistical analysis ($p > 0.05$) indicated that there was no statistically significant difference between the measured depths and the actual depths across all slope categories.

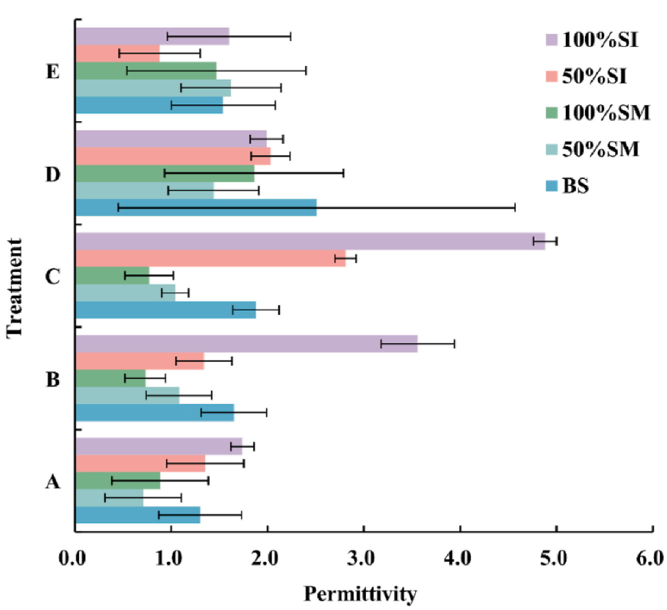

Fig. 6. Difference of permittivity between black soil and loess parent materials under different treatments. Group A: bulk density of 1.1 g cm^{-3}, moisture content of 20 %; Group B: bulk density of 1.3 g cm^{-3}, moisture content of 20 %; Group C: bulk density of 1.5 g cm^{-3}, moisture content of 20 %; Group D: bulk density of 1.3 g cm^{-3}, moisture content of 10 %; Group E: bulk density of 1.3 g cm^{-3}, moisture content of 30 %. LPM: loess parent material; BS: bare slope; SM: straw-mulched slope; SI: straw-incorporated slope.

3.3. Distribution of black soil thickness under straw return conditions

The continuous variation in black soil thickness along the slope under different soil conservation tillage is illustrated in Fig. 7. The average black soil thicknesses of the bare slope, straw-mulched slope, and straw-incorporated slope were 29.1 cm, 28.6 cm, and 34.6 cm, respectively. Overall, the black soil thickness on the bare slope exhibited an increasing trend from the slope summit to the slope toe, with a thickness range of 16.4–48.7 cm. The thickness variation trends observed across the three measurement lines along the slope were generally consistent. Notably, near the 38 m slope length position, the black soil thickness showed a marked increase, with the average thickness attaining 31.6 cm. At approximately 120 m along the slope length, the thickness of the black soil was relatively thin, averaging 27.7 cm. After the slope length reached 160 m, the soil layer thickness exhibited a gradual increase, attaining an average thickness of 34.9 cm. The distribution of black soil thickness on the straw-mulched slope was uneven, with a fluctuation range of 20.0–46.6 cm. Notably, certain segments of the slope, specifically within the 40–60 m and 100–120 m intervals along its length, demonstrated comparatively greater soil thickness. In contrast, soil thickness remained relatively stable across other positions of the slope. Within the slope length range of 60–100 m in the middle of the slope, the black soil thickness was relatively thin, with an average thickness of 26.6 cm. From a slope length of 150 m extending toward the slope toe, the black soil thickness exhibited a gradual increase, attaining an average thickness of 30.7 cm. The overall variation range of black soil thickness on the straw-incorporated slope was 19.3–48.6 cm. At the slope summit (0–20 m), the soil layer was notably thin, averaging 25.9 cm in thickness. Subsequently, as the slope length increased, the black soil thickness demonstrated a pattern characterized by an initial increase, followed by a decrease, and then a subsequent increase. From 40 to 60 m along the slope length, the black soil thickness continuously increased, attaining 35.8 cm. Subsequently, extending to approximately 110 m slope length, the change in black soil thickness became stable and decreased to

Table 2
Actual buried depth of iron pipes and measured depth by GPR on different slopes.

Sample plot	Actual depth (cm)	GPR measurement (cm)	Accuracy (%)	*p*
Bare soil	30	28.8 ± 1.7	96.1	0.99
	27	25.6 ± 1.8	95.0	
	30	29.3 ± 2.2	97.7	
Straw-mulched slope	22	23.4 ± 0.9	93.8	0.97
	30	26.4 ± 1.7	88.1	
	31	26.8 ± 1.0	86.5	
Straw-incorporated slope	28	25.1 ± 1.4	89.5	0.98
	41	36.1 ± 0.9	88.1	
	39	35.8 ± 1.2	91.9	

Note: $p > 0.05$ indicates no significant difference.

31.9 cm. Near the toe of the slope, a slight increase in thickness was observed, reaching 33.3 cm.

4. Discussion

4.1. Impact of straw return practices and soil properties on the permittivity

This study systematically revealed the influence patterns of conservation tillage practices, specifically straw mulching and straw incorporation, and basic soil properties (moisture content, bulk density) on the soil permittivity. The findings derived from the SEM analysis demonstrated that soil moisture content and bulk density exerted positive influences on soil permittivity, aligning broadly with prior research outcomes (Koyama et al., 2017; Luo et al., 2019). Under straw mulching conditions, soil bulk density and moisture content exerted a more significant impact than the straw mulching rate. This suggests that, within this management practice, the intrinsic physical characteristics of the soil predominantly govern variations in permittivity. Significantly, both the straw mulching rate and the straw incorporation rate demonstrated a negative impact on the soil permittivity. This effect is ascribed to the porous nature of the straw, which likely alters electromagnetic wave interactions with the soil matrix. Similar to studies showing that porous biochar derived from straw enhances microwave reflection loss via increased scattering and absorption (Aslam et al., 2021; Zou et al., 2024), the inherent porosity of raw straw may reduce electromagnetic wave penetration efficiency through analogous mechanisms, consequently leading to a lower measured soil permittivity. The modulation of permittivity by the porosity of straw can be understood through two primary mechanisms. First, the incorporation of air, which possesses a low permittivity, leads to a direct reduction in the overall permittivity of the straw-soil composite medium. Second, within a heterogeneous porous system, the scattering of electromagnetic waves and alterations in the effective propagation pathways further impact the measured permittivity values (Huang et al., 2014).

Under conditions of straw incorporation, a significant alteration was observed in the hierarchical influence of controlling factors. The findings indicated that the rate of straw incorporation became the primary determinant affecting variations in soil permittivity, exerting a pronounced direct negative impact that exceeded the effect of soil moisture content. This phenomenon highlights the fundamental distinction between the mechanisms through which straw incorporation and straw mulching influence the soil: when straw is chopped and evenly integrated into the soil, it no longer functions solely as a surface modification but significantly transforms the soil characteristics. The interaction between plentiful straw fragments and soil particles results in the formation of a "composite medium" characterized by unique electromagnetic properties, which markedly diminishes the overall dielectric response (Tran et al., 2022). SEM analysis revealed that the incorporation of straw modified the composition and microstructure of the medium, consequently affecting the sensitivity of permittivity to variations in bulk density. Under these conditions, the dielectric properties were primarily governed by the quantity of straw incorporated and the resultant structural porosity generated by its presence.

In our study, independent control over the bulk density of the soil layer under conditions involving straw incorporation was not achievable. Following the addition of straw, the bulk density of the soil layer exhibited deviations from the predetermined target value. To address this limitation, future investigations should employ more refined methodologies, such as separately quantifying the volumetric proportions of soil and added materials within the composite medium, or utilizing computed tomography (CT) scanning techniques to characterize the microstructural properties of the composite medium. Simultaneously, the regulatory role of soil texture in the relationship between straw return and permittivity cannot be overlooked. Soils with different textures, such as sand, loam, and clay, exhibit substantial differences in pore structure and particle composition. Clay particles, as charged solid phases, influence the solid-phase dielectric properties of soil. An increase in clay content alters these properties and induces dielectric loss, consequently leading to a reduction in soil permittivity (González-Teruel et al., 2020).

4.2. Effectiveness and limitations of GPR applications

This study conducted a systematic assessment of the feasibility of using GPR to detect the black soil thickness under varying straw return practices. The findings demonstrated that, under conditions involving straw return, there was a significant difference in permittivity between the black soil and the underlying loess parent material (Table 1). Specifically, under the gradients of moisture content and bulk density designed in this experiment, the straw incorporation treatment (especially 100 % SI) exhibited a significant difference ($p < 0.05$) in permittivity between the black soil and loess parent material, indicating that GPR could effectively detect black soil thickness. It is important to note that under conditions of elevated moisture content (Group E: 30 %), the treatment involving 50 % incorporation did not exhibit a statistically significant difference from the loess parent material, thereby constraining the efficacy of GPR detection. Consequently, it is advisable to perform surveys when the field moisture content is below 30 % to enhance detection performance. Regarding straw mulching, no significant difference from loess parent material was observed under conditions of low bulk density (Group A: 1.1 g cm^{-3}) or low moisture content (Group D: 10 %), which adversely affects the accuracy of GPR detection. The attenuation of electromagnetic wave intensity caused by the mulch layer and its

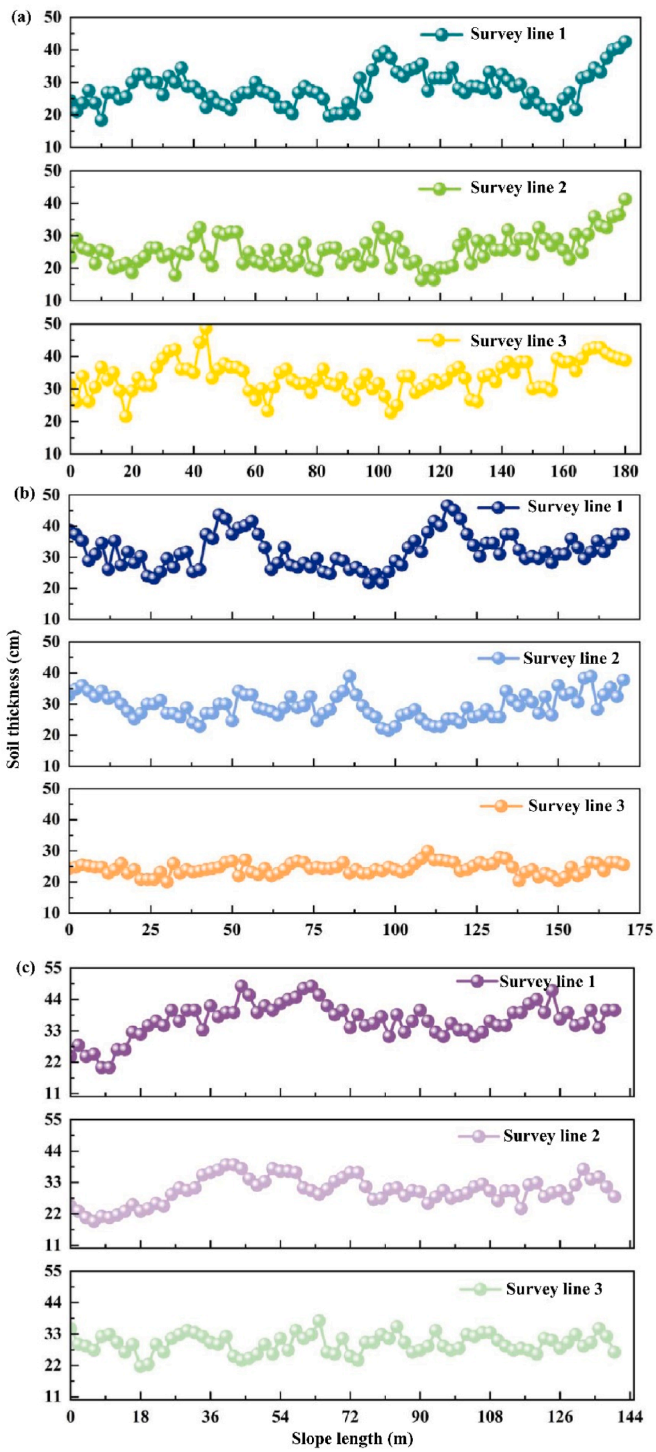

Fig. 7. Variation of black soil thickness on slopes: (a) bare slope; (b) straw-mulched slope; (c) straw-incorporated slope.

impact on dielectric permittivity are comparatively minimal (Wang et al., 2022b). Based on a comparative analysis conducted across varying experimental gradients, it is recommended to regulate or select a soil moisture content within the range of 20 % to 30 % when utilizing GPR for soil thickness assessments in the context of straw return practices. This moisture range effectively mitigates the adverse effects associated with excessively dry conditions and enhances the reliability of detection. However, under conditions of excessive soil moisture exceeding 30 %, additional investigation is warranted to elucidate the impact of medium electrical conductivity on the propagation of electromagnetic waves.

The findings of this study may provide a useful reference for other regions characterized by black soil or loam with comparable soil textures, climatic conditions, and agricultural practices. However, for areas exhibiting significant differences in soil texture (sandy soils), straw type (rice or wheat straw), or climatic regimes, it is advisable to perform localized, small-scale calibration prior to the direct application of the quantitative parameters identified herein, such as the optimal moisture content range. Various application contexts impose distinct demands on precision. For instance, regional soil resource surveys and mapping endeavors seek to acquire a broad-scale comprehension of the spatial distribution of soil thickness, typically utilizing low-to medium-resolution data (50–100 m) (Malone et al., 2017), which allows for a comparatively large margin of error. The accuracy achieved by the proposed method adequately satisfies these requirements, facilitating an efficient and non-destructive alternative to numerous conventional borehole measurements, as well as enabling rapid delineation of spatial variability in soil thickness. Within the domain of precision agricultural management, the requisite level of accuracy is considerably more stringent (Minasny & McBratney, 2016). The present error margin associated with our methodology, ranging from 6.2 % to 13.5 %, may be nearing the threshold of its applicability for these purposes. The GPR technique for estimating soil thickness under straw return conditions, validated in this study, demonstrates adequate accuracy for dependable use in applications such as soil resource assessments and large-scale agricultural management. In these contexts, the benefits of the method, including that it causes no damage, acquires data rapidly, and supports continuous measurement, can be effectively leveraged. However, for engineering projects or precision agronomic practices that require high absolute accuracy, it is advisable to combine GPR surveys with a limited number of calibration boreholes in order to improve absolute accuracy through localized calibration.

Laboratory experiments are limited in their ability to accurately reproduce the complex conditions present in field environments. At broader spatial scales, variables including soil texture, moisture content, bulk density, and the spatial distribution of straw demonstrate significant heterogeneity, with variability levels substantially greater than those attainable within controlled soil box settings. This disparity can influence the propagation behavior of GPR signals, thereby reducing the accuracy of practical field measurements. Furthermore, owing to the limitations associated with extensive destructive sampling, our study utilized only nine soil profiles to validate the accuracy of GPR. This restricted sample size may contribute to uncertainty in the estimation of the absolute detection accuracy of GPR. It is recommended that future investigations adopt a more densely distributed, grid-based validation framework over broader spatial extents. Our study primarily focused on the initial stage of straw return. Future research should investigate the long-term effects of straw return on soil dielectric properties, particularly the distinct contributions of fresh plant residues versus humified organic matter. In recent years, GPR has been applied to geological structure investigations and is emerging as an increasingly common tool for various near-surface applications. However, electromagnetic waves undergo undesirable scattering in heterogeneous structures, which reduces resolution or detection depth (Takahashi et al., 2015). The impact of straw return on soil dielectric properties was elucidated in this study. Consequently, a scientific basis is provided for the precise interpretation of GPR data in farmland management.

In future applications, it is essential to incorporate region-specific straw return practices along with fundamental soil characteristics to optimize detection timing or to perform targeted calibration of GPR data. This approach is expected to significantly enhance the accuracy and reliability of GPR technology when used in complex media environments, such as farmland with straw return.

5. Conclusions

This study systematically investigated the variation characteristics of the soil dielectric constant under straw return conditions and evaluated the feasibility of using GPR to determine the thickness of black soil in the presence of straw return, through a combination of indoor simulation experiments and field detection. It should be noted that the field validation of our study is based on a limited number of points, which may affect the universality of the accuracy conclusions. Under straw return conditions, the accuracy range of GPR in determining black soil thickness was 86.5 %–93.8 %, with an average accuracy of 91.86 % $\pm$ 3.78 %, effectively enabling the detection of black soil thickness under straw return conditions.

However, for straw-mulched conditions, GPR exhibited limitations in effectively differentiating the black soil layer from the parent material layer, particularly when the bulk density was low (1.1 g cm^{-3}) and moisture content was minimal (10 %). In contrast, the performance of GPR improved under conditions characterized by medium to high bulk density and moderate to high moisture content. Under straw-mulched conditions, the factors affecting the soil permittivity were ranked as follows: moisture content, bulk density, and straw-mulched rate. In contrast, under straw-incorporation conditions, the order of influence was incorporation rate, moisture content, and bulk density. Meanwhile, bulk density and moisture content had a positive effect on the permittivity, whereas the rates of straw mulching and straw incorporation exhibited negative effects.

The distribution of black soil thickness along the slope varied according to the different straw return techniques employed. On the bare slope, the black soil thickness generally showed an increasing trend from 27.9 cm at the slope top to 34.9 cm at the slope toe. On the straw-mulched slope, the thickness distribution was uneven, with localized peaks reaching up to 46.6 cm. The soil layer in the middle of the slope was relatively thin (26.6 cm), and the thickness increased to 30.7 cm at the slope bottom. For the straw-incorporated slope, the soil thickness exhibited a fluctuating pattern of “increase-decrease-increase” along the slope length. The soil thickness change in the middle of the slope was relatively stable, with a slight increase to 33.3 cm at the slope bottom.

CRediT authorship contribution statement

Chang Liu: Writing – original draft, Methodology, Investigation, Formal analysis, Conceptualization. **Gang Liu:** Writing – review & editing, Supervision, Methodology, Investigation, Funding acquisition, Formal analysis. **Chenxi Dan:** Investigation. **Ya Liu:** Investigation. **Qiong Zhang:** Investigation. **Han Luo:** Investigation. **Chutian Zhang:** Investigation. **Zhen Guo:** Investigation. **Kaishan Song:** Investigation.

Declaration of competing interest

The authors declare that they have no known competing financial interests or personal relationships that could have appeared to influence the work reported in this paper.

Acknowledgements

This research was supported by the National Key R&D Program of China (No. 2024YFD1501104), the Strategic Priority Research Program of the Chinese Academy of Sciences (No. XDA28010201), and the Natural Science Basic Research Plan in Shaanxi Province (No. 2024JC-JCQN-39).

References

Afshar, F. A., Ayoubi, S., Castrignanò, A., Quarto, R., & Mahmoudzadeh Ardekani, M. R. (2017). Using ground-penetrating radar to explore the cemented soil horizon in an arid region in Iran. *Near Surface Geophysics, 15*, 103–110. https://doi.org/10.3997/1873-0604.2016049

Aslam, M. A., Ding, W., ur Rehman, S., Hassan, A., Bian, Y., Liu, Q., & Sheng, Z. (2021). Low cost 3D bio-carbon foams obtained from wheat straw with broadened bandwidth electromagnetic wave absorption performance. *Applied Surface Science, 543*, Article 148785. https://doi.org/10.1016/j.apsusc.2020.148785

Ebraheem, M. O., Ibrahim, H. A., & Zalat, M. M. (2025). Revealing the past of Ginah archaeological site by enhancing GPR images to understand ancient periods at Kharga Oasis, Egypt. *Scientific Reports, 15*(1), Article 26478. https://doi.org/10.1038/s41598-025-10570-5

Eckmeier, E., Gerlach, R., Gehrt, E., & Schmidt, M. W. I. (2007). Pedogenesis of chernozems in Central Europe - A review. *Geoderma, 139*(3-4), 288–299. https://doi.org/10.1016/j.geoderma.2007.01.009

González-Teruel, J. D., Jones, S. B., Soto-Valles, F., Torres-Sánchez, R., Lebron, I., Friedman, S. P., & Robinson, D. A. (2020). Dielectric spectroscopy and application of mixing models describing dielectric dispersion in clay minerals and clayey soils. *Sensors, 20*(22), 6678. https://doi.org/10.3390/s20226678

Huang, Y., Wang, Y., Li, Z., Yang, Z., Shen, C., & He, C. (2014). Effect of pore morphology on the dielectric properties of porous carbons for microwave absorption applications. *Journal of Physical Chemistry C, 118*(45), 26027–26032. https://doi.org/10.1021/jp506999k

Jonard, F., Mahmoudzadeh, M., Roisin, C., Weihermüller, L., André, F., Minet, J., Vereecken, H., & Lambot, S. (2013). Characterization of tillage effects on the spatial variation of soil properties using ground-penetrating radar and electromagnetic induction. *Geoderma, 207*, 310–322. https://doi.org/10.1016/j.geoderma.2013.05.024

Kan, Z.-R., Virk, A. L., He, C., Liu, Q.-Y., Qi, J.-Y., Dang, Y. P., Zhao, X., & Zhang, H.-L. (2020). Characteristics of carbon mineralization and accumulation under long-term conservation tillage. *Catena, 193*, Article 104636. https://doi.org/10.1016/j.catena.2020.104636

Kassam, A., Friedrich, T., & Derpsch, R. (2019). Global spread of conservation agriculture. *International Journal of Environmental Studies, 76*(1), 29–51. https://doi.org/10.1080/00207233.2018.1494927

Koyama, C. N., Liu, H., Takahashi, K., Shimada, M., Watanabe, M., Khuut, T., & Sato, M. (2017). In-situ measurement of soil permittivity at various depths for the calibration and validation of low-frequency SAR soil moisture models by using GPR. *Remote Sensing, 9*(6), 580. https://doi.org/10.3390/rs9060580

Labaz, B., Hartemink, A. E., Zhang, Y., Stevenson, A., & Kabala, C. (2024). Organic carbon in mollisols of the world - A review. *Geoderma, 447*, Article 116937. https://doi.org/10.1016/j.geoderma.2024.116937

Labaz, B., Musztyfaga, E., Waroszewski, J., Bogacz, A., Jezierski, P., & Kabala, C. (2018). Landscape-related transformation and differentiation of chernozems - Catenary approach in the Silesian lowland, SW Poland. *Catena, 161*, 63–76. https://doi.org/10.1016/j.catena.2017.10.003

Lal, R. (2013). Enhancing ecosystem services with no-till. *Renewable Agriculture and Food Systems, 28*(2), 102–114. https://doi.org/10.1017/S1742170512000452

Li, X., Zeng, L., Zhu, L., Jiang, H., Liu, C., & Dai, Y. (2025). Strong adsorption of tetracycline on carbon blacks: An in-depth study of the adsorption mechanism. *Journal of Water Process Engineering, 70*, Article 106784. https://doi.org/10.1016/j.jwpe.2024.106784

Liu, C., Liu, G., Li, H., Wang, X., Chen, H., Dan, C., Shen, E., & Shu, C. (2021). Using ground-penetrating radar to investigate the thickness of mollic epipedons developed from loessial parent material. *Soil and Tillage Research, 212*, Article 105047. https://doi.org/10.1016/j.still.2021.105047

Luo, G., Cao, Y., Bai, Z., Huang, Y., & Wang, S. (2019). Soil bulk density difference, ground penetrating radar feature identification, and simulation for a reclaimed soil profile in the dumping site of an open pit mine. *Journal of Agricultural and Resource Economics, 36*(4), 441–452. https://doi.org/10.13254/j.jare.2018.0286 (*In Chinese*).

Malone, B. P., Styc, Q., Minasny, B., & McBratney, A. B. (2017). Digital soil mapping of soil carbon at the farm scale: A spatial downscaling approach in consideration of measured and uncertain data. *Geoderma, 290*, 91–99. https://doi.org/10.1016/j.geoderma.2016.12.008

Marecos, V., Solla, M., Fontul, S., & Antunes, V. (2017). Assessing the pavement subgrade by combining different non-destructive methods. *Construction and Building Materials, 135*, 76–85. https://doi.org/10.1016/j.conbuildmat.2017.01.003

Minasny, B., & McBratney, A. B. (2016). Digital soil mapping: A brief history and some lessons. *Geoderma, 264*, 301–311. https://doi.org/10.1016/j.geoderma.2015.07.017

Nearing, M. A., Xie, Y., Liu, B., & Ye, Y. (2017). Natural and anthropogenic rates of soil erosion. *International Soil and Water Conservation Research, 5*(2), 77–84. https://doi.org/10.1016/j.iswcr.2017.04.001

Pathirana, S., Lambot, S., Krishnapillai, M., Cheema, M., Smeaton, C., & Galagedara, L. (2024). Integrated ground-penetrating radar and electromagnetic induction offer a non-destructive approach to predict soil bulk density in boreal podzolic soil. *Geoderma, 450*, Article 117028. https://doi.org/10.1016/j.geoderma.2024.117028

Persico, R. (2014). *Introduction to ground penetrating radar: Inverse scattering and data processing* (p. 400). Hoboken, NJ: John Wiley & Sons, Inc..

Rosegrant, M. W., & Cline, S. A. (2003). Global food security: Challenges and policies. *Science, 302*(5652), 1917–1919. https://doi.org/10.1126/science.1092958

Soil Survey Staff. (2010). *Keys to soil taxonomy, eleventh edition*. Washington, DC: USDA-Natural Resources Conservation Service.

Song, F., Liu, M., Qi, Z., Zhang, Z., Wang, B., Yin, Z., Xu, J., & Sun, J. (2024). Straw returning and reducing nitrogen application rates maintain maize yields and reduce gaseous nitrogen emissions from black soil maize fields. *Applied Soil Ecology, 203*, Article 105637. https://doi.org/10.1016/j.apsoil.2024.105637

Sorokin, A., Owens, P., Láng, V., Jiang, Z.-D., Michéli, E., & Krasilnikov, P. (2021). "Black soils" in the Russian soil classification system, the US soil taxonomy and the WRB: Quantitative correlation and implications for pedodiversity assessment. *Catena, 196*, Article 104824. https://doi.org/10.1016/j.catena.2020.104824

Steelman, C. M., & Endres, A. L. (2012). Assessing vertical soil moisture dynamics using multi-frequency GPR common-midpoint soundings. *Journal of Hydrology, 436–437*, 51–66. https://doi.org/10.1016/j.jhydrol.2012.02.041

Sui, J., & Dai, Y. (2025). Analysis of conservation practices for Black soil based on organic matter and nitrogen contents in the black soil region of Northeast China. *Scientific Reports, 15*(1), Article 23989. https://doi.org/10.1038/s41598-025-09426-9

Sun, W., Canadell, J. G., Yu, L., Yu, L., Zhang, W., Smith, P., Fischer, T., & Huang, Y. (2020). Climate drives global soil carbon sequestration and crop yield changes under conservation agriculture. *Global Change Biology, 26*, 3325–3335. https://doi.org/10.1111/gcb.15001

Takahashi, K., Igel, J., Preetz, H., & Sato, M. (2015). Sensitivity analysis of soil heterogeneity for ground-penetrating radar measurements by means of a simple modeling. *Radio Science, 50*(2), 79–86. https://doi.org/10.1002/2014RS005499

Tong, Y., Liu, J., Li, X., Sun, J., Herzberger, A., Wei, D., … Zhang, F. (2017). Cropping system conversion led to organic carbon change in China's Mollisols regions. *Scientific Reports, 7*(1), Article 18064. https://doi.org/10.1038/s41598-017-18270-5

Tran, T. T. T., Dao, T. T., Dinh, V. M., Vu, T. T. T., Nguyen, H. T., Nguyen, P. M., … Nguyen, M. N. (2022). Effects of microsized rice straw on soil clay dispersibility. *European Journal of Soil Science, 73*(3), Article e13246. https://doi.org/10.1111/ejss.13246

Wang, W., Deng, X., & Yue, H. (2024). Black soil conservation will boost China's grain supply and reduce agricultural greenhouse gas emissions in the future. *Environmental Impact Assessment Review, 106*, Article 107482. https://doi.org/10.1016/j.eiar.2024.107482

Wang, Y., Qiao, J., Ji, W., Sun, J., Huo, D., Liu, Y., & Chen, H. (2022b). Effects of crop residue managements and tillage practices on variations of soil penetration resistance in sloping farmland of mollisols. *International Journal of Agricultural and Biological Engineering, 15*(1), 164–171. https://doi.org/10.25165/j.ijabe.20221501.6526

Wang, H., Yang, S., Wang, Y., Gu, Z., Xiong, S., Huang, X., Sun, M., Zhang, S., Guo, L., Cui, J., Tang, Z., & Ding, Z. (2022a). Rates and causes of black soil erosion in Northeast China. *Catena, 214*, Article 106250. https://doi.org/10.1016/j.catena.2022.106250

Wu, J., Teng, B., Zhong, Y., Duan, X., Gong, L., Guo, W., Qi, P., Haider, F. U., & Cai, L. (2024). Enhancing soil aggregate stability and organic carbon in northwestern China through straw, biochar, and nitrogen supplementation. *Agronomy, 14*(5), 899. https://doi.org/10.3390/agronomy14050899

Xiao, L. G., Kuhn, N. J., Zhao, R. Q., & Cao, L. H. (2021). Net effects of conservation agriculture principles on sustainable land use: A synthesis. *Global Change Biology, 27*(24), 6321–6330. https://doi.org/10.1111/gcb.15906

Xie, Y., Tang, J., Gao, Y., Gu, Z. J., Liu, G., & Ren, X. Y. (2023). Spatial distribution of soil erosion and its impacts on soil productivity in Songnen typical black soil region. *International Soil and Water Conservation Research, 11*(4), 649–659. https://doi.org/10.1016/j.iswcr.2023.01.002

Yang, J., Liu, H., Lei, T., Rahma, A. E., Liu, C., & Zhang, J. (2021). Effect of straw-incorporation into farming soil layer on surface runoff under simulated rainfall. *Catena, 199*, Article 105082. https://doi.org/10.1016/j.catena.2020.105082

Zhang, S., Chen, X., Jia, S., Liang, A., Zhang, X., Yang, X., … Zhou, G. (2015). The potential mechanism of long-term conservation tillage effects on maize yield in the black soil of Northeast China. *Soil and Tillage Research, 154*, 84–90. https://doi.org/10.1016/j.still.2015.06.002

Zhang, X., Dao, L., Zhang, C., Morrison, L., Hong, B., Zhang, H., & Gan, Y. (2018). Mapping the spatial distribution of soil depth in a grassland ecosystem with the aid of ground penetrating radar and GIS (Northwestern Sichuan, China). *Grassland Science, 64*(4), 217–225. https://doi.org/10.1111/grs.12201

Zhang, J., Li, Y., Yuan, J., Chi, F., Kuang, E., Zhu, Y., … Liu, J. (2024). Analysis of the fluorescence spectral characteristics of dissolved organic matter in a black soil with different straw return amounts. *Scientific Reports, 14*, Article 29948. https://doi.org/10.1038/s41598-024-72050-6

Zou, L., Peng, C., Zhuo, Y., Liang, F., Liu, Z., & Chen, J. (2024). Rice straw-inspired tunable multi-hollow channel parallel carbon fibers for enhanced electromagnetic wave absorption. *Carbon, 227*, Article 119240. https://doi.org/10.1016/j.carbon.2024.119240